

Search for Hybrid Baryons with CLAS12 in Hall B
(Dated: April 14, 2016)

Contents

A. Run condition	2
B. Count rates from $K^+\Lambda$	5
C. Monte-Carlo studies of the for hybrid baryon manifestation in exclusive KY electroproduction	6
D. Photocoupling extraction	7
E. TODO	10

A. Run condition

We are planning to search the hybrid state at low Q^2 and the accessible range of Q^2 depends on the beam energy and torus current. Another issue that affects the selection of the best run condition is that we need good particle momentum resolution to be able to separate Λ and Σ^0 electroproduction channels and the better resolution is achieved with larger torus current. The Λ and Σ^0 separation is based on using the cuts on the missing mass of kaon. For this purpose kaon must be detected. Thus, we have to use the topologies when the final state electron, kaon and at least one of the other hadrons (p or π^+) are detected.

The run condition studies were performed with fact MC. The results are shown in Figs. 1 and 2. Table I summarizes the relevant information for different run conditions. The best run conditions correspond to the large negative torus currents, as the maximal Λ and Σ^0 separation is achieved and the gap in the Q^2 coverage is small.

TABLE I: Minimal achievable Q^2 (Q_{min}^2) and the percentage of the Λ and Σ^+ events that can be isolated from each other at different run conditions.

E_{beam} , GeV	Tor. current, A	Q_{min}^2 , GeV ²	Λ separation, %	Σ^0 separation, %
6.6	+1500	0.05	33	19
6.6	-1500	0.05	86	73
6.6	+3700	0.05	32	19
6.6	-3700	0.05	100	100
8.8	+1500	0.1	21	8
8.8	-1500	0.1	31	16
8.8	+3700	0.1	16	8
8.8	-3700	0.1	100	100

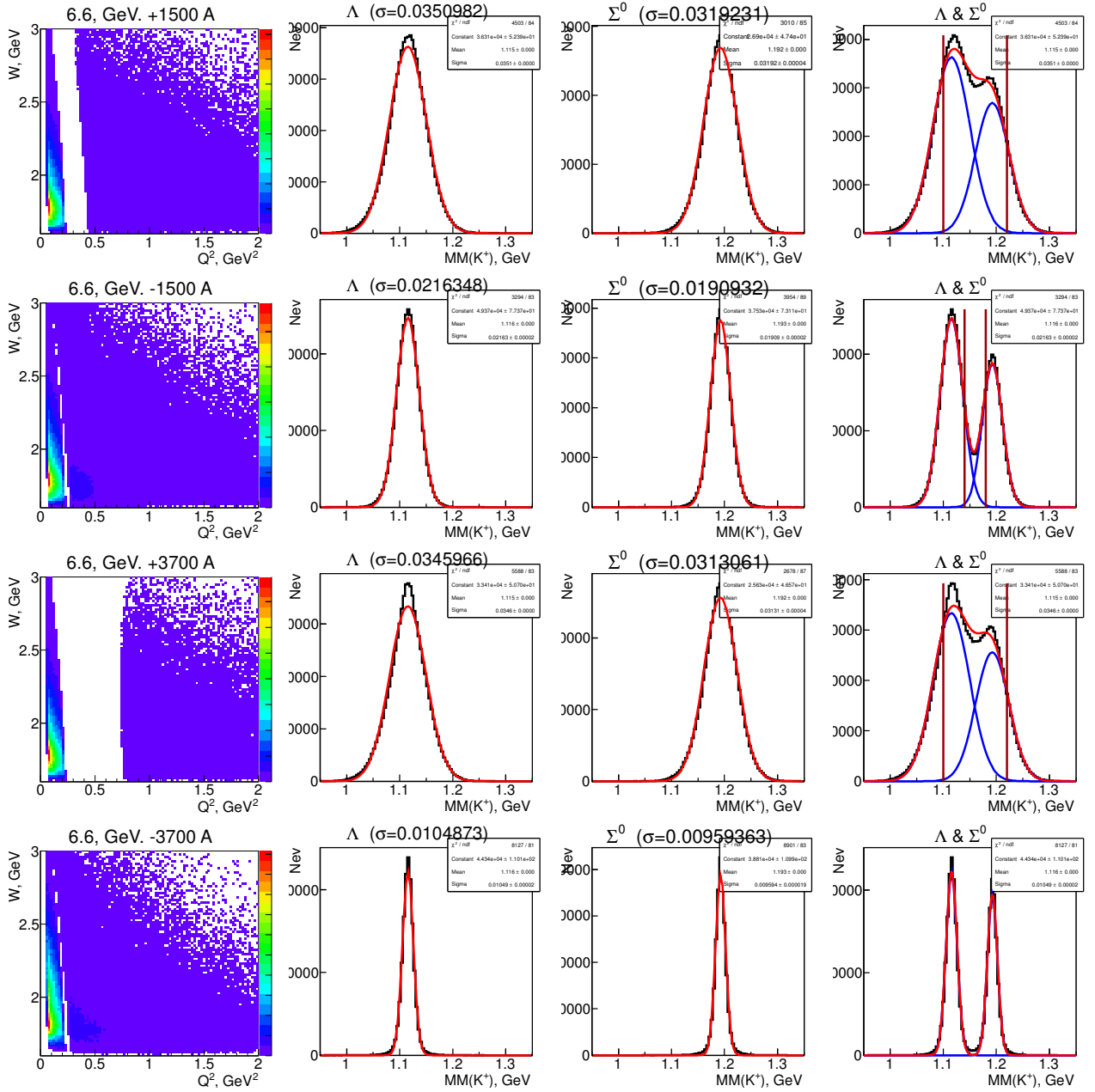


FIG. 1: The left column shows the W versus Q^2 distributions at different torus currents for $Q^2 < 2 \text{ GeV}^2$ when the beam energy is 6.6 GeV. Next three columns show the distributions of the missing mass off K^+ for the corresponding torus current. The vertical lines indicate the cuts to be used to separate Λ or Σ^0 from its neighboring state. When no lines are drawn then Λ and Σ^0 are fully separated.

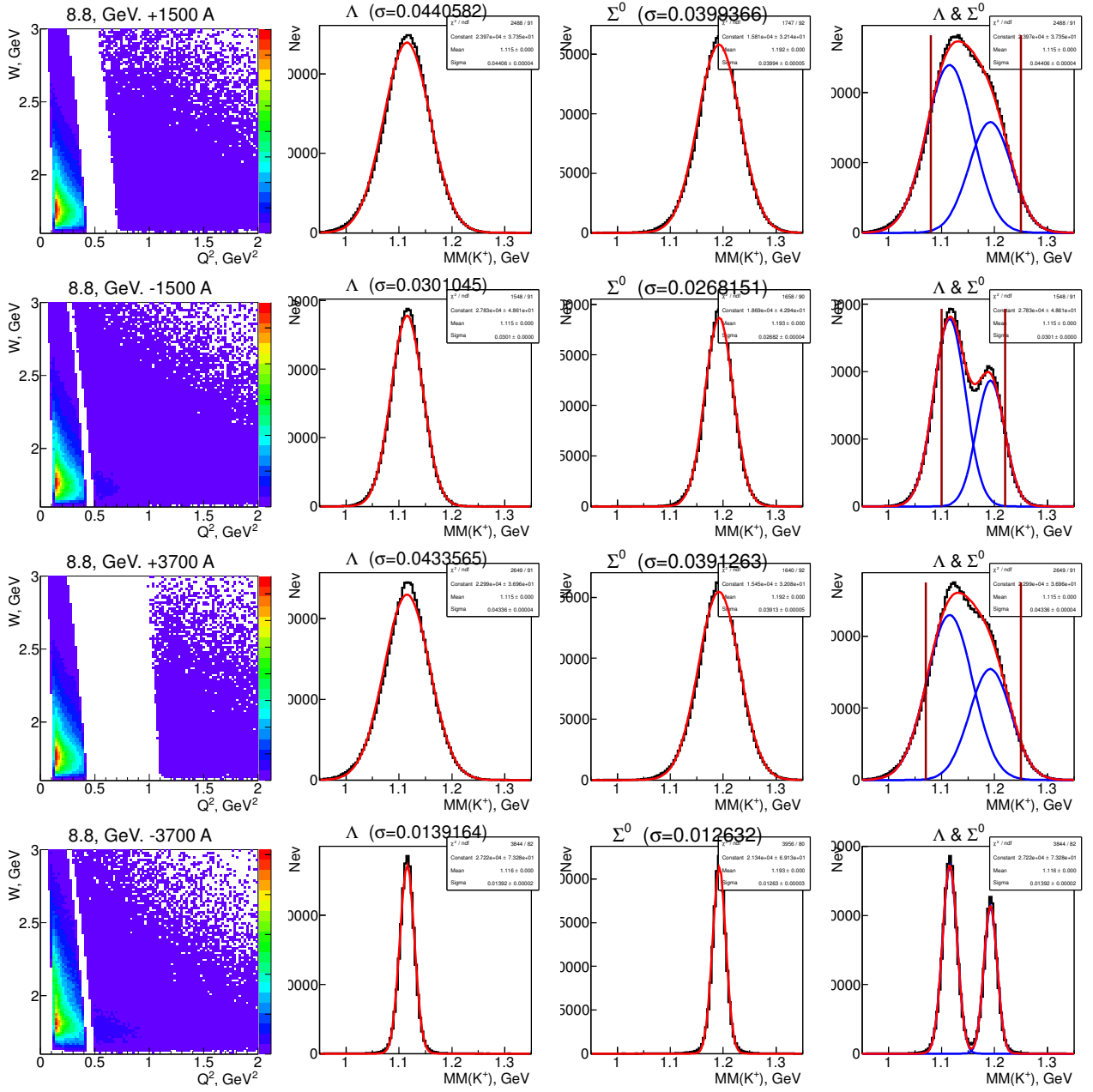


FIG. 2: The left column shows the W versus Q^2 distributions at different torus currents for $Q^2 < 2 \text{ GeV}^2$ when the beam energy is 8.8 GeV. Next three columns show the distributions of the missing mass off K^+ for the corresponding torus current. The vertical lines indicate the cuts to be used to separate Λ or Σ^0 from its neighboring state. When no lines are drawn then Λ and Σ^0 are fully separated.

B. Count rates from $K^+\Lambda$

...To add at the end of the section “Count rates from $K^+\Lambda$ ”...

... The maximal total event rate is therefore expected to be $240 \times 100 = 24$ kHz for the trigger condition described above.

...Should we add the next paragraph as a kind of cross check for the count rate calculation?

The count rate also can be estimated in the following way. Suppose, the maximal inclusive event rate is 20 KHz, which is limited by the data acquisition. Then under the rough assumption that Λ event rate is about 1% with respect to the inclusive event rate we can estimate the Λ event rate to be ≈ 200 Hz. This number is in a reasonable coincidence with the previously obtained value of 240 Hz.

However, the studies in the section A showed that the preferable run conditions are achieved if using large negative torus currents, as Λ and Σ^0 can be fully separated.

The rate of the “separated” Λ or Σ^0 events when the beam energy is 6.6 GeV and the torus current is -1500 A is expected to be $240 \text{ Hz} \times 86\% \approx 200 \text{ Hz}$ (see section A). When the beam energy is 6.6 GeV and the torus current is -1500 A the same rate is $112 \text{ Hz} \times 100\% \approx 100 \text{ Hz}$. However, we have to take into account: first the total event rate of 24 kHz may not be feasible due to the limitations of the data acquisition and secondly the momentum resolution may differ from what is predicted by fast MC, and in this case the percentage of the separated Λ or Σ^0 events can become smaller.

The obtained event rate should be reduced by 8%, as 8% of the events do not have reconstructed kaon and by 34%, since the Λ decay branching fraction to the channel (p, π^-) is 64%. Assuming the Λ electroproduction rate is 100 Hz, we expect to collect in 40 days of the beam time $100 \text{ Hz} \times 34\% \times 64\% \times 40 \text{ days} \approx 2 \times 10^8$ events.

C. Monte-Carlo studies of the for hybrid baryon manifestation in exclusive KY electroproduction

an addition to the section “Planned Monte-Carlo studies ...”. This section should be modified, as it is not a plan, it has been done.

Formula (4) should be modified. $\Gamma_{\lambda_f} = \frac{1}{2}\Gamma_r, 0.03$ I used 3% branching fraction.

The paragraph just before formula (9) and the subsequent text should be modified to take into account the acceptance. Further is my modification...

In order to quantify the statistical significance of the difference between the exclusive KY event distributions over the θ_K , ϕ_K CMS angles as simulated according to the models A and B, the following χ^2 definition will be used:

$$\chi^2 = \frac{1}{N_{d.p.}} \sum_{W, \cos(\theta_K), \phi_K} \frac{\left(\frac{d^2\sigma_A}{d\Omega_K} - \frac{d^2\sigma_B}{d\Omega_K} \right)^2}{\delta^2}, \quad (1)$$

where $\frac{d^2\sigma_A}{d\Omega_K}$ and $\frac{d^2\sigma_B}{d\Omega_K}$ are the cross sections simulated in the models A and B, respectively.

The χ^2 is evaluated in each Q^2 bin independently and we choose 0.1 GeV² bin with in Q^2 . The sum over W in (1) run from $M_R - \Gamma_R/2$ to $M_R + \Gamma_R/2$ and the bin width in W is 20 MeV. We used 24 bins in $\cos(\theta_K)$ and ϕ_K . Assuming that the statistical uncertainties dominate, the uncertainties for the differences $\left(\frac{d^2\sigma_A}{d\Omega_K} - \frac{d^2\sigma_B}{d\Omega_K} \right)$ between the event distributions simulated in the models B and A, respectively, can be evaluated as:

$$\delta^2 = \left(\frac{\frac{d^2\sigma_A}{d\Omega_K}}{\sqrt{N_A}} \right)^2 + \left(\frac{\frac{d^2\sigma_B}{d\Omega_K}}{\sqrt{N_B}} \right)^2, \quad (2)$$

where N_A and N_B are the number of events in three dimensional bins in W and Ω_K for the models A and B, respectively.

The number of events in the mentioned above three dimensional bins for a given bin in Q^2 can be calculated knowing the expected total number of events in the whole covered kinematic space. The number of events in each multidimensional bin is proportional to the cross section in that bin taking acceptance into account. The cross section $\frac{d^2\sigma}{d\Omega_K}$ are obtained by integrating over the other kinematic variables: final state electron azimuthal angle ϕ_e and spherical angles of the one of the Λ decay product particles, say proton, θ_p , ϕ_p . Assume that the cross section $\frac{d^5\sigma}{d\Omega_K d\phi_e d\theta_p d\phi_p}$ does not depend on ϕ_e , θ_p and ϕ_p . Then the number of events (N) in every four dimensional bin is

$$N(Q^2, W, \theta_K, \phi_K) = C \int_{\phi_e, \theta_p, \phi_p} a \times \frac{d^5\sigma}{d\theta_K d\phi_K d\phi_e d\theta_p d\phi_p} = C \int_{\phi_e, \theta_p, \phi_p} a \times \frac{d^2\sigma}{d\Omega_K} \approx C \sum_{\phi_e, \theta_p, \phi_p} a \times \frac{d^2\sigma}{d\Omega_K}, \quad (3)$$

where a is the CLAS12 acceptance and it depends on all kinematic variables. C is a constant. Set the sum of all $N(Q^2, W, \theta_K, \phi_K)$ equal to the expected total number of events in the whole kinematic covered space we find the constant C .

The number of evens in each multidifferential bin was calculated assuming the total number of $K\Lambda$ events to be collected in the experiment is 2×10^8 (see section B).

D. Photocoupling extraction

The photocouplings can be extracted by comparing the model cross section to the experimental one, as it was described in the section C. The expected number of events in multidimensional bins were calculated as described in the same section. The typical number of events in one bin of the single differential distribution $\frac{d\sigma}{d\cos(\theta_K)}$ is about few thousands and the statistical errors are negligible, while in two fold differential distribution $\frac{d^2\sigma}{d\Omega_K}$ statistical errors are meaning. This can be seen in Figs. 3 through 6

We define the the minimal value of the photocoupling such as it is the minimal value of the photocoupling when the χ^2 from (1) characterizing the difference between two cross sections is more than 4. The minimal values of A_{12} , A_{32} and S_{12} found in this way are presented in Tables II and III. The mass of the hybrid state was 2.2 GeV and the total width was 0.250 GeV. The Q^2 bin width was 0.1 GeV².

TABLE II: The minimal values of the photocouplings for the beam energy 6.6 GeV and the torus current -2950 A for the resonances with the spin (J_R) 1/2 and 3/2. A_{12} , A_{32} and S_{12} are in the units of $10^{-3}\times\text{GeV}^{-1/2}$. When determining the minimal value of A_{12} we varied only A_{12} setting the other photocouplings to zero. The minimal values of A_{32} and S_{12} were obtained in the same way.

Q^2 , GeV ²	$J_R=1/2$		$J_R=3/2$		
	A_{12}	S_{12}	A_{12}	A_{32}	S_{12}
0.1	12	12	16	11	10
0.5	17	19	18	19	12
1.0	16	21	16	18	10

TABLE III: The minimal values of the photocouplings for the beam energy 8.8 GeV and the torus current -2950 A for the resonances with the spin (J_R) 1/2 and 3/2. A_{12} , A_{32} and S_{12} are in the units of $10^{-3}\times\text{GeV}^{-1/2}$. When determining the minimal value of A_{12} we varied only A_{12} setting the other photocouplings to zero. The minimal values of A_{32} and S_{12} were obtained in the same way.

Q^2 , GeV ²	$J_R=1/2$		$J_R=3/2$		
	A_{12}	S_{12}	A_{12}	A_{32}	S_{12}
0.3	12	12	14	12	9
0.5	19	20	19	21	12
1.0	16	21	16	18	9

It was found that the minimal photocoupling values are weakly dependent on the run conditions and Q^2 . The weak dependence on Q^2 can be explained. The resonance manifestation is more pronounced at small Q^2 , as the non-resonant background is smaller, on the other hand statistical errors are larger (the same Q^2 bin width (0.1 GeV²) is used at all Q^2) and the sensitivity to the resonance gets smaller. These two factor works in opposite direction and the χ^2 does not change significantly.

Figs. 3 through 6 present examples of the comparison of the model to the model plus resonance one- and two fold differential cross sections. The model plus resonance cross section was calculated when the photocoupling was set to its minimal value from the Table III.

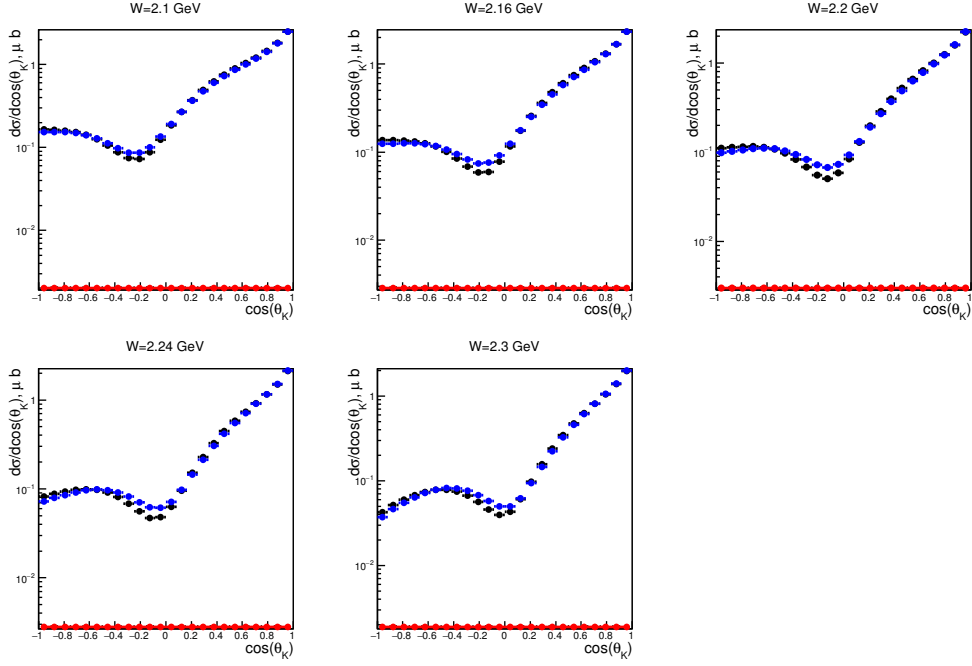


FIG. 3: Comparison of the model cross section $d\sigma/d\cos(\theta_K)$ (black points) with the model plus resonance cross section (blue points) for the beam energy 8.8 GeV and the torus current -2950 A at $Q^2=0.3$ GeV² and at few values of W . The cross section of the resonance contribution is shown in red. The spin of the resonance is 1/2 and the A_{12} is $12\times 10^{-3}\text{GeV}^{-1/2}$, it corresponds to the minimal A_{12} from the table III. Statistical errors are negligible.

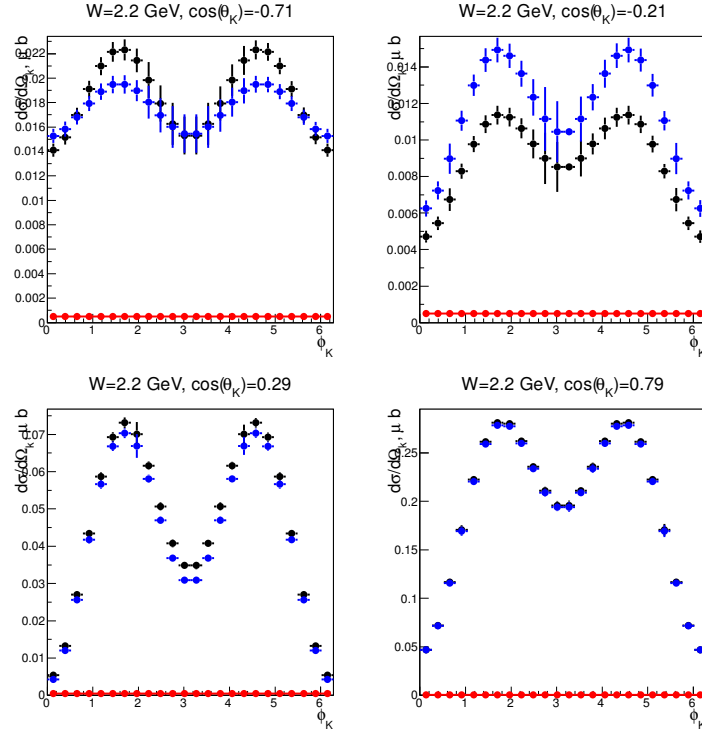


FIG. 4: Comparison of the model cross section $d\sigma/d\Omega(\theta_K)$ with the model plus resonance cross section at $W = M_R$ and few values of $\cos(\theta_K)$. The same conditions run condition and Q^2 as in Fig. 3. The errors are statistical.

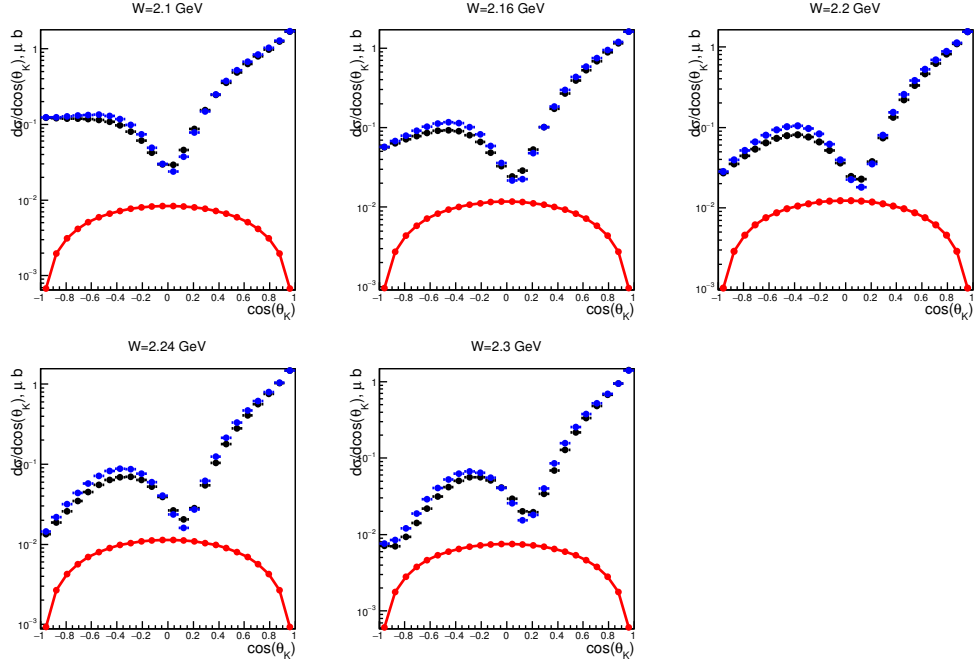


FIG. 5: Comparison of the model cross section $d\sigma/d\cos(\theta_K)$ (black points) with the model plus resonance cross section (blue points) for the beam energy 8.8 GeV and the torus current -2950 A at $Q^2=0.3$ GeV² and at few values of W . The cross section of the resonance contribution is shown in red. The spin of the resonance is 3/2 and the A_{32} is $18 \times 10^{-3} \text{ GeV}^{-1/2}$, it corresponds to the minimal A_{32} from the table III. Statistical errors are negligible.

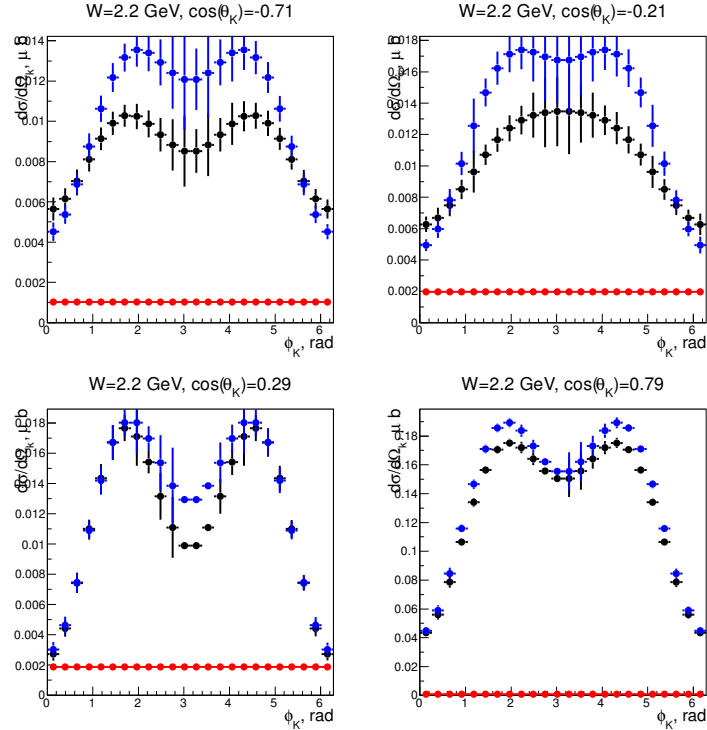


FIG. 6: Comparison of the model cross section $d\sigma/d\Omega(\theta_K)$ with the model plus resonance cross section at $W = M_R$ and few values of $\cos(\theta_K)$. The same conditions run condition and Q^2 as in Fig. 5. The errors are statistical.

E. TODO

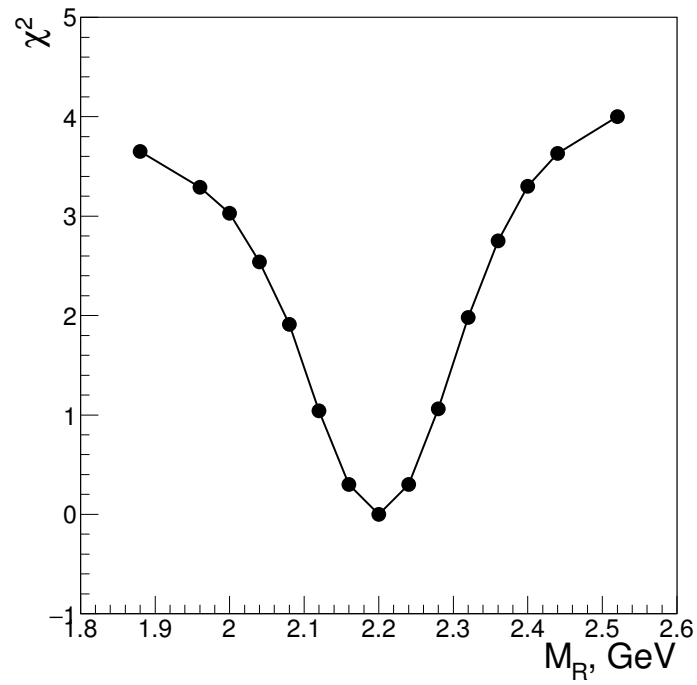


FIG. 7: ...

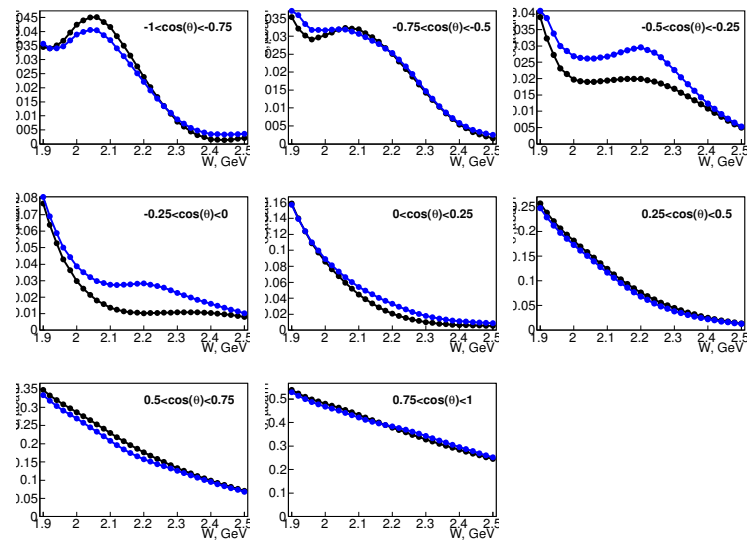


FIG. 8: ...